nature materials

LETTERS

PUBLISHED ONLINE: 14 NOVEMBER 2010 | DOI: 10.1038/NMAT2893

Direct observation of the temporal and spatial dynamics during crumpling

Hillel Aharoni and Eran Sharon*

Crumpling occurs when a thin deformable sheet is crushed under an external load or grows within a confining geometry. Crumpled sheets have large resistance to compression and their elastic energy is focused into a complex network of localized structures[1]. Different aspects of crumpling have been studied theoretically[2,3], experimentally[4,5] and numerically[6,7]. However, very little is known about the dynamic evolution of three-dimensional spatial configurations of crumpling sheets. Here we present direct measurements of the configurations of a fully elastic sheet evolving during the dynamic process of crumpling under isotropic confinement. We observe the formation of a network of ridges and vertices into which the energy is localized. The network is dynamic. Its evolution involves movements of ridges and vertices. Although the characteristics of ridges agree with theoretical predictions, the measured accumulation of elastic energy within the entire sheet is considerably slower than predicted. This could be a result of the observed network rearrangement during crumpling.

In the process of crumpling, an initially flat sheet is increasingly confined, resulting in its deformation. This deformation incorporates bending and stretching of the sheet, the energy of which is given by elastic plate theory. Crumpling is an example of an energy focusing behaviour: certain confining geometries, including isotropic ones, lead to the nucleation of geometrical defects within the sheet. For an ideally elastic, infinitely thin sheet, the energy density within these defects diverges. For any physical sheet, it is regularized by sheet thickness, grain size or plasticity effects. By studying crumpling at a macroscopic scale, we can gain insight into the dynamics and evolution of energy focusing and the regularization of these singularities. Crumpling also demonstrates the transition of a deterministic system into a complex state, which is typically not its global energy minimum and is characterized only by its statistical properties. A simplification to the elastic problem which enables theoretical progress assumes that all the energy of the sheet is stored in localized high energy structures in the form of vertices and ridges[1]. To estimate the total elastic energy we need to know the energy within a single stress focusing structure, and the distribution of these structures. Previous theoretical and experimental works have investigated the focusing properties of isolated ridges[3,8] and vertices (d cones)[9,10]. The statistics of the ridge ensemble were calculated on the basis of a ridge-breaking scenario: as confinement increases new vertices are nucleated within existing ridges, dividing them into smaller ridges[11].

Experimental verification of the theoretical predictions is partial. In most experiments materials were not purely elastic, resulting in localization of plastic deformation in ridges and cones. Such plastic 'scars' were used to retrospectively analyse patterns in opened crumpled sheets[4,12]. However, the actual three-dimensional (3D) configuration of a crumpled sheet was never measured. Mechanical and geometrical properties of the crumpled state were deduced indirectly from force[5], pressure[13] or acoustic emission measurements[14,15]. The accumulation of energy as a function of confinement was found to be slower than theoretically predicted[5]. Friction and plasticity were suggested as possible origins for this effective softness of the crumpled state. Recent numerical simulations provided some insight as for the actual configuration of a crumpled sheet, with and without plasticity[6,7]. Interestingly, it was found that, as in ref. 5, the accumulation of elastic energy was slower than was predicted theoretically. The origin of this effective softness is a key question in crumpling.

We make direct real-time measurements of the geometry of weakly crumpled sheets in 3D space and associate it with the material (Lagrangian) coordinates. These are measured in an elastic sheet as it crumples under isotropic confinement. We use temperature-responsive elastic gel sheets that controllably swell inside a fixed boundary, rather than fixed-size sheets that are placed inside a collapsing boundary. Gel discs of initial thickness $h_0 = 130\,\mu\mathrm{m}$ and diameter $L_0 = 5\,\mathrm{cm}$ are inserted into a hollow glass sphere (Fig. 1), which provides the rigid-spherical-confinement conditions. The sphere is filled with water, which is density matched with the gel to eliminate gravitational effects, and is placed inside a temperature-controlled tank. The sheet initially adopts an approximately flat configuration. We then slowly cool down the tank ($\sim 1\,^{\circ}\mathrm{C\,h^{-1}}$). As the sheet is cooled down its diameter gradually increases, thus exceeding the inner diameter of the sphere, forcing the sheet to start crumpling. The compaction ratio $\eta \equiv L/L_s$ (ratio between the sheet's rest diameter L and the sphere's diameter L_s) is increased to $\eta_{max} \approx 1.6$. Owing to the gel's isotropic expansion, the Föppl–von Kármán number $\gamma \equiv (L/h)^2 = (L_0/h_0)^2 \approx 1.5 \times 10^5$ remains constant. Our sheets are polymerized together with yellow fluorescent powder and red fluorescent beads. The homogeneous distribution of the powder makes the gel fluorescent. The beads are embedded within the sheet and remain at fixed positions within it, thus serving as Lagrangian tracers during crumpling. As the sheet swells we repeatedly scan it using laser tomography, obtaining its 3D configuration from the gel fluorescence. In addition, we obtain the 3D positions of individual tracers embedded in the gel. As we also have the initial two-dimensional (2D) Lagrangian coordinates of each tracer, these data enable us to calculate the embedding function of the sheet for each η (see Methods). Using these embedding functions we calculate the local metric and the local mean ($H \equiv (1/2)(\kappa_1 + \kappa_2)$) and Gaussian ($K \equiv \kappa_1\kappa_2$) curvatures ($\kappa_1$ and κ_2 are the local principal curvatures). The elastic-bending-energy density is given by $\varepsilon_b \propto Yh^3\beta$ where Y is Young's modulus and $\beta \equiv 4H^2 - K$ the bending content density. This relation holds for a constant Poisson ratio of 1/2, which is applicable in our case. The total bending energy of the sheet is given by $E_b = \int \varepsilon_b \mathrm{d}^2x = Yh^3 \int \beta \mathrm{d}^2x$. The dimensionless scale-invariant bending content $B = \int \beta \mathrm{d}^2x$ is

[1]The Racah Institute of Physics, The Hebrew University of Jerusalem, 91904, Israel. *e-mail: erans@vms.huji.ac.il.

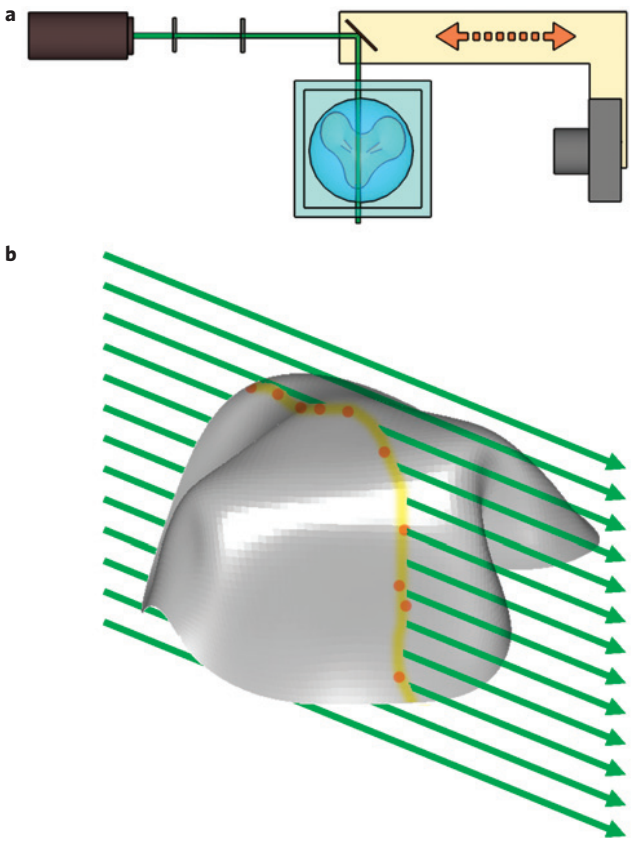

Figure 1 | Experimental system. a, Top view. A gel sheet is placed inside a glass spherical shell, immersed in a temperature-controlled tank, and illuminated by a moving laser plane. **b**, The sheet contains fluorescent powder and tracer particles that emit light (yellow and red respectively) at the intersection curve of the sheet and the laser plane. Images of multiple slices are captured by a co-moving camera. The 3D configuration of the sheet is reconstructed using the (yellow) fluorescence induced in the gel. The positions of the individual (red) tracers embedded in the gel provide a Lagrangian coordinate system (see Methods).

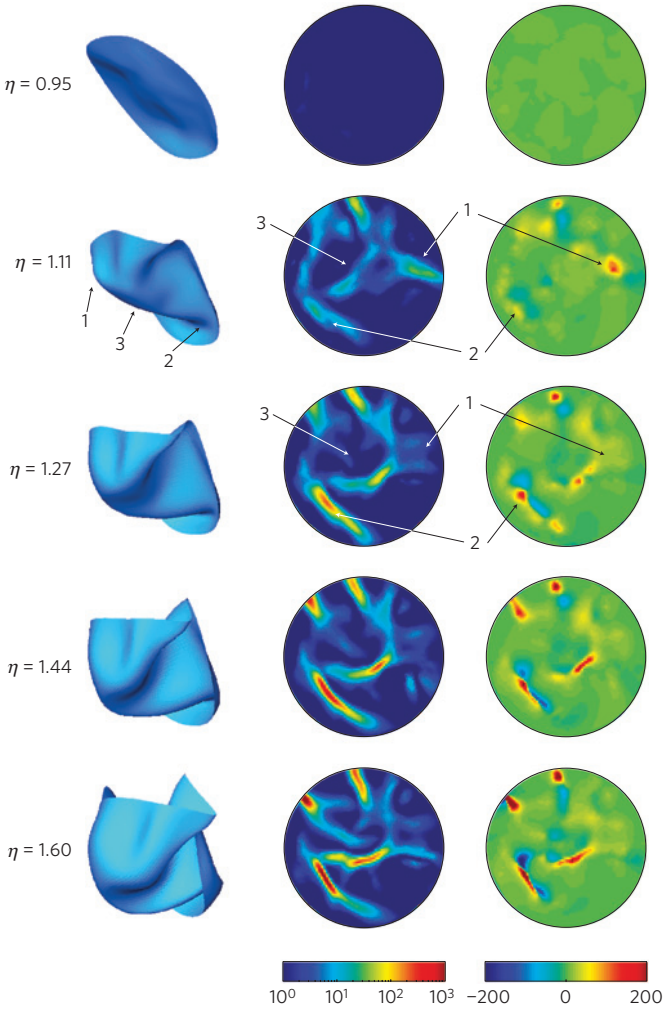

Figure 2 | Evolution of crumpling. 3D configuration of the crumpling sheet (left), bending-content density, β (centre), and Gaussian curvature distribution (right), viewed in the disc (Lagrangian) coordinates, at increasing compaction ratios ($\eta \equiv L/L_s$). 1 and 2 mark specific vertices whereas 3 marks a ridge (see the text). Both colour bars are in units of L_s^{-2}.

proportional to the total bending energy, but is determined only by the geometry of the sheet, and can therefore be calculated directly from the embedding function.

In Fig. 2 we see the evolution of a single crumpling sheet. The figure shows the 3D shape of the sheet (left) at increasing compaction ratios (see also Supplementary Movie S1). Also shown are the bending-content density (centre) and the Gaussian curvature distribution (right) in 2D Lagrangian coordinates, in units of L_s^{-2} (L_s is the sphere's diameter). As the sheet is confined, the initial flat configuration (top) evolves into an increasingly complex 3D configuration (bottom). Despite the isotropy and homogeneity of the experiment, energy is localized into a network of narrow structures (centre column; note the logarithmic colour scale). These structures are comprised of ridges and vertices, indicating the existence of a crumpled state even at these low confinement ratios. The Gaussian curvature (right-hand column) is localized mainly at isolated spots at the vertices. Localized regions of positive Gaussian curvature (red) are accompanied by regions of negative Gaussian curvature (blue), forming 'curvature dipoles'. This local compensation of curvature was also observed in simulations of a single d cone[16]. The development of the stress-focusing network involves rich dynamics; it includes movement and disappearance of distinct stress foci (for example marks 1 and 2 in Fig. 2), as well as variations in the strength of existing structures. We suggest that such rearrangement is an important process in crumpling of elastic sheets.

We turn to examine the characteristics of energy focusing within the individual objects that compose the network. We look at the relation between values of bending-content density β and the area fraction ϕ (from a selected region) that contains such energy density or higher[17]. Focusing profiles of $\beta \propto \phi^{-1}$ and $\beta \propto \phi^{-0.8}$ were predicted for a single isolated vertex and ridge respectively. Additionally, cutoffs for both low and high area fractions were predicted and observed numerically[17]. We plot the focusing profiles for ridge-like and cone-like structures within the sheet (Fig. 3a). For the ridge structure the focusing profile is well described by a power law $\beta \propto \phi^{-0.8\pm0.1}$, which is consistent with theoretical predictions. The scaling spans over 1.5 decades, with the anticipated cutoffs. For the cone structure the behaviour does not seem to obey a power law; nevertheless, the focusing profile is steeper than that of the ridge.

We now turn to examine the focusing profile of the entire sheet. In Fig. 3b we show the bending-energy-density profiles for an entire sheet in different compaction ratios. The power-law regime of the profile widens with increasing compaction ratio, penetrating more and more into the low-fraction regime. This is a first direct quantitative measurement of energy focusing in a crumpling sheet. The profiles seem to approach an asymptotic power-law behaviour

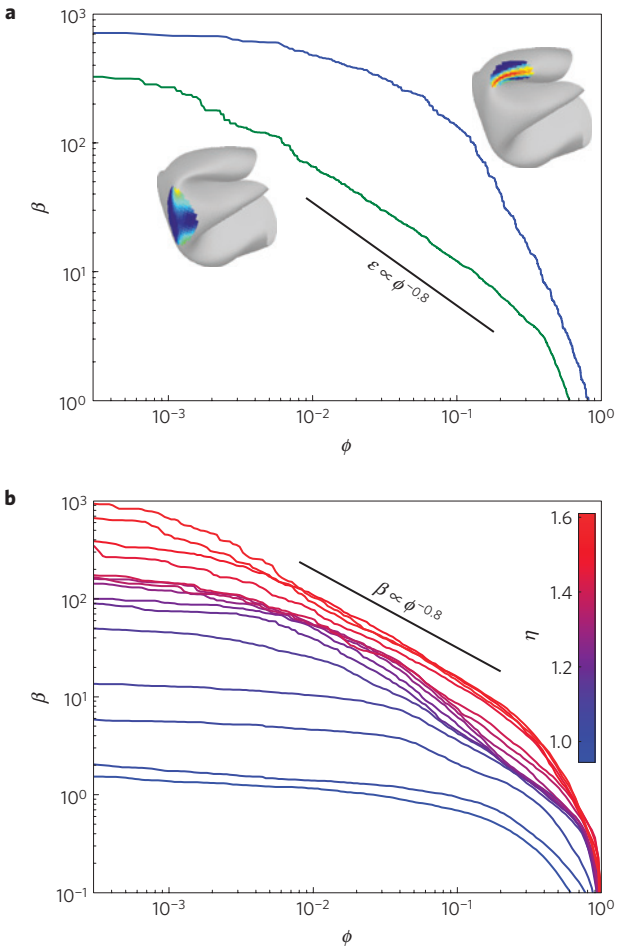

Figure 3 | Bending-content-density profiles. a, Profiles for the region around a vertex (blue curve) and around a ridge (green curve). The highlighted parts on the 3D surfaces show the regions of interest. The solid black line is the theoretically predicted relation for an isolated ridge. **b**, Profiles of the entire sheet for increasing (equally spaced) compaction ratios (blue to red). The profiles approach −0.8 scaling for increasing η.

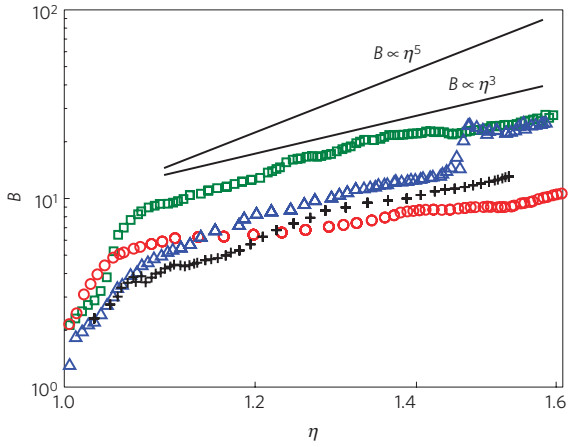

Figure 4 | Accumulation of bending content during compaction. The log–log plot shows the bending content in the sheet as a function of compaction ratio for four different experiments under the same conditions. Solid black lines show η^5 (theoretical prediction) and η^3 scaling for comparison. The 'jump' in the blue curve at $\eta \approx 1.45$ is a result of a ridge-breaking event.

with a power of approximately −0.8, as in the case of a single ridge. This provides an extra indication of the dominant role of ridges in the focusing of energy during crumpling[1]. This dominancy is already apparent in low compaction ratios.

Next we examine the accumulation of bending energy in an increasingly confined sheet. Theoretically derived scaling relations for the energy[1] translate to $B = \gamma^a \eta^b$ for the (dimensionless) bending content B. Here $\gamma \equiv (L/h)^2$ and $\eta \equiv L/L_s$ are the sheet's Föppl–von Kármán number and compaction ratio respectively. The theoretical analysis predicts $a = 1/6$ and $b = 5$ for self-avoiding sheets in the highly confined regime. In our experiment B is directly measured and γ is constant.

The dependence of the bending content on the compaction ratio η is shown in Fig. 4 for four selected experiments. As the crumpling sheet is not in a global minimal-energy state, different experiments result in different curves. All curves, however, exhibit an accumulation rate that is significantly slower than the predicted $B \propto \eta^5$ (shown in the figure). The data are best fitted by a $B \propto \eta^{3\pm0.2}$ relation, starting at compaction ratios as low as $\eta \approx 1.1$. This is consistent with recent numerical simulations[6,18], which have reported a relation $B \propto \eta^3$ (shown in the figure) for isotropic confinements over a large range of compaction ratios, starting at low compaction ratios as in our experiments. Measurements corresponding to an exponent of $b \sim 2.5$ were reported for a mylar sheet crushed by a piston[5], where it was suggested that plastic effects could be the origin of the deviation from the theoretical predictions. Our experiments show that, even for elastic sheets under isotropic confinement, conditions that are similar to those assumed by the theoretical analysis, crumpled sheets are much softer than they are theoretically predicted to be.

We have already shown that the energy is indeed contained mainly in ridges, and that theory correctly predicts the energy focusing within each of them (Fig. 3). Nevertheless, the theory overestimates the accumulation of energy within the entire sheet. Theoretical analysis of crumpling evolution often assumes that the network is frozen and only refines as compaction is increased (hierarchical breaking)[11]. We have already pointed out (Fig. 2) that the network is dynamic rather than frozen. We thus turn to analyse the dynamics within the sheet during crumpling. In Fig. 5a we present the bending-content density at four (Lagrangian) points as a function of compaction ratio. Some of the points undergo phases of decrease in their local bending-content density. This demonstrates that, during compaction, there is a rich spatial and temporal dynamics; existing objects move or fade and their motion gives rise to violent fluctuations in the local energy density. To learn how this dynamics affects the evolution of the crumpled state we need to measure the local energy variations and characterize their statistics.

Although for the whole sheet (Fig. 4) the energy accumulation exponent $y \equiv (d(\log B))/(d(\log \eta))$, $B \propto \eta^y$, is positive and constant, from Fig. 5a it is evidently not so locally. To gain insight into the length scales related to the rearrangement processes we analyse the evolution of the bending content B_r enclosed within regions of different sizes r. We compute the local rate of change $y_r \equiv (d(\log B_r))/(d(\log \eta))$ for 2,000 randomly selected windows of radius r (in Lagrangian coordinates) from the power-law regime $(1.1 < \eta < 1.4)$. Probability distribution functions of y_r for different window sizes r are shown in Fig. 5b. All distributions are shifted towards positive values, as expected because the sheets are being confined and thus continuously gain elastic energy. For small window sizes the distributions are nearly symmetric and decay slowly (roughly exponentially; see the inset). In addition, they contain many negative values, indicating an abundance of local relaxation processes. As the window size increases negative values become rare and the probability distribution functions become narrower and increasingly asymmetric. This indicates that the relaxation processes are only local and do not involve relaxation

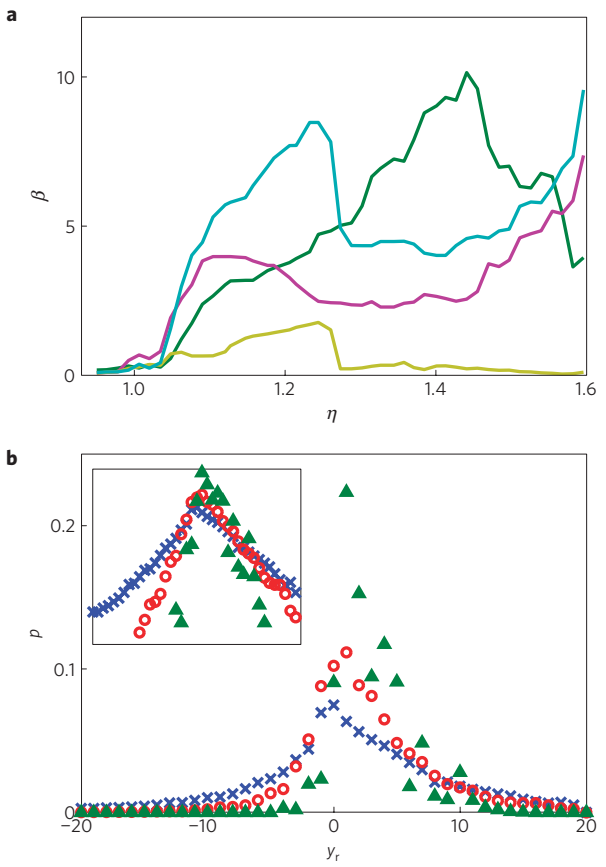

Figure 5 | Local stress relaxation within the sheet. a, Bending-content density at four different points on the sheet as a function of compaction ratio. Events of local energy decrease can be seen. **b**, Probability distribution functions of y_r (local change rate of the bending content as a function of η, within radius r) for three different radii (cross, 0.02; open circle, 0.14; filled triangle, 0.52 of the sheet's diameter). For smaller r the occurrence of negative values of y_r increases, reflecting the local nature of energy rearrangement and relaxation within the sheet. Inset, A semi-log plot. For smaller r the distribution's decay is roughly exponential.

of the entire sheet. The underlying dynamics may involve both movement of energy foci and changes in their strength. For example, in Fig. 2 the vertex marked 1 significantly weakens whereas vertex 2 strengthens. Simultaneously, the location of ridge 3 varies as the sheet crumples. Although the movement of energy foci was previously observed in an elastic sheet under a point load[19–21], we know of no such observations in a crumpled sheet. We note that these rearrangements and movements are expected to be repressed in the presence of plasticity.

In conclusion, we have presented direct measurements of the dynamics of crumpling of an isotropically confined elastic sheet. We have shown that the bending-energy distribution within a single ridge is consistent with theoretical predictions, and that the energy distribution in the entire crumpled sheet becomes ridge dominated early in the crumpling process. The accumulation of bending energy with increasing confinement is slower than predicted by theoretical models of crumpling, indicating 'softness' of the crumpled state. Finally, we have shown that the evolution of a crumpled state involves extensive movement and rearrangement of energy foci. These elastic processes allow for local energy relaxation that can partly account for the softness of the system. Our experiment suggests that crumpling can be studied as an evolving system in which defect rearrangement, and not just nucleation, plays an important role.

Methods

We use elastic thermo-responsive hydrogel discs made of polymerized *N*-isopropylacrylamide with nanoclay composites[22]. The sheet is of initial (at 35 °C) diameter $L_0 = 5$ cm and thickness $h_0 = 130$ μm. The sheet is seeded with red fluorescent beads of 107 μm diameter, and evenly dyed with yellow fluorescent powder. The sheet is inserted into an $L_S = 5.5$-cm-diameter hollow glass sphere filled with water, which is density matched to the gel by addition of 4% sodium polytungstate. The glass sphere is immersed in a temperature-regulated water bath. The system is cooled from 35 °C at a rate of ∼1 °C h^{-1} to 25 °C, resulting in the sheet's swelling and hence crumpling. The maximal compaction ratio (at 25 °C) is $\eta_{max} \approx 1.6$.

Tomography of the sheet's 3D configuration is carried out using a green (532 nm Nd:YAG) laser plane, which illuminates a series of ∼250 parallel slices (with ∼250 μm spacing) of the sphere. Each full scan lasts ∼30 s, much shorter than the typical timescale for configuration changes under the applied cooling rate. The fluorescent scattering from each slice is captured by a co-moving 5 MP colour camera that is positioned perpendicularly to the laser plane. We use a sharp low-pass filter that blocks the wavelength of the laser. The fluorescence is captured by the camera and the bead (red) and powder (yellow) signals are extracted from its different colour channels.

The 3D shape of the entire surface is obtained from the tomogram of the fluorescent gel sheet. However, the type of analysis we wish to apply requires identification of the material (Lagrangian) coordinates on the sheet. This we acquire using the data from the beads; the typical distance between beads (∼3 mm) is larger than the maximum displacement of individual beads between consecutive scans, thus enabling 3D particle tracking of the beads (approximately 200 beads) from the initial flat configuration. In the flat configuration we easily assign 2D material coordinates to each particle, which remain the same throughout the measurement because the particles are entrapped within the gel. We thus identify the position in 3D space of each set of 2D material coordinates at each η. The 2D coordinate network is further refined by interpolating (using surface geodesics) between points of known Lagrangian coordinates, thus giving us a fine (≈100 × 100 grid) 2D → 3D mapping of the sheet at each η.

The mapping which identifies each set of material coordinates with its actual position in space is known as the embedding function. The embedding function contains all the information regarding the deformation of the sheet. We use the embedding function to calculate the metric, bending scalars and bending-energy density, and assign them to the appropriate 2D material coordinates. This enables both detection of object movement on the sheet and assignment of an appropriate measure to each area element for correct integration of local quantities.

Received 17 February 2010; accepted 24 September 2010; published online 14 November 2010

References

1. Witten, T. A. Stress focusing in elastic sheets. *Rev. Mod. Phys.* **79,** 643–675 (2007).
2. Ben Amar, M. & Pomeau, Y. Crumpled paper. *Proc. Math. Phys. Eng Sci.* **453,** 729–755 (1997).
3. Lobkovsky, A., Gentges, S., Li, H., Morse, D. & Witten, T. A. Scaling properties of stretching ridges in a crumpled elastic sheet. *Science* **270,** 1482–1485 (1995).
4. Plouraboué, F. & Roux, S. Experimental study of the roughness of crumpled surfaces. *Physica A* **227,** 173–182 (1996).
5. Matan, K., Williams, R. B., Witten, T. A. & Nagel, S. R. Crumpling a thin sheet. *Phys. Rev. Lett.* **88,** 076101 (2002).
6. Vliegenthart, G. A. & Gompper, G. Forced crumpling of self-avoiding elastic sheets. *Nature Mater.* **5,** 216–221 (2006).
7. Tallinen, T., Åström, J. A. & Timonen, J. The effect of plasticity in crumpling of thin sheets. *Nature Mater.* **8,** 25–29 (2009).
8. Venkataramani, S. C. Lower bounds for the energy in a crumpled elastic sheet—a minimal ridge. *Nonlinearity* **17,** 301–312 (2004).
9. Cerda, E., Chaïeb, S., Melo, F. & Mahadevan, L. Conical dislocations in crumpling. *Nature* **401,** 46–49 (1999).
10. Chaïeb, S., Melo, F. & Géminard, J. Experimental study of developable cones. *Phys. Rev. Lett.* **80,** 2354–2357 (1998).
11. Sultan, E. & Boudaoud, A. Statistics of crumpled paper. *Phys. Rev. Lett.* **96,** 136103 (2006).
12. Blair, D. L. & Kudrolli, A. Geometry of crumpled paper. *Phys. Rev. Lett.* **94,** 166107 (2005).
13. Lin, Y. C., Wang, Y. L., Liu, Y. & Hong, T. M. Crumpling under an ambient pressure. *Phys. Rev. Lett.* **101,** 125504 (2008).
14. Kramer, E. M. & Lobkovsky, A. E. Universal power law in the noise from a crumpled elastic sheet. *Phys. Rev. E* **53,** 1465–1469 (1996).
15. Houle, P. A. & Sethna, J. P. Acoustic emission from crumpling paper. *Phys. Rev. E* **54,** 278–283 (1996).
16. Wang, J. W. & Witten, T. A. Compensation of Gaussian curvature in developable cones is local. *Phys. Rev. E* **80,** 046610 (2009).

17. DiDonna, B. A., Witten, T. A., Venkataramani, S. C. & Kramer, E. M. Singularities, structures, and scaling in deformed m-dimensional elastic manifolds. *Phys. Rev. E* **65,** 016603 (2001).
18. Tallinen, T., Åström, J. A. & Timonen, J. Deterministic folding in stiff elastic membranes. *Phys. Rev. Lett.* **101,** 106101 (2008).
19. Boudaoud, A., Patricio, P., Couder, Y. & Ben Amar, M. Dynamics of singularities in a constrained elastic plate. *Nature* **407,** 718–720 (2000).
20. Vaziri, A. & Mahadevan, L. Localized and extended deformations of elastic shells. *Proc. Natl Acad. Sci. USA* **105,** 7913–7918 (2008).
21. Das, M., Vaziri, A., Kudrolli, A. & Mahadevan, L. Curvature condensation and bifurcation in an elastic shell. *Phys. Rev. Lett.* **98,** 014301 (2007).
22. Haraguchi, K., Takehisa, T. & Fan, S. Effects of clay content on the properties of nanocomposite hydrogels composed of poly(*N*-isopropylacrylamide) and clay. *Macromolecules* **35,** 10162–10171 (2002).

Acknowledgements

We thank G. Cohen for assisting in writing this paper. This work was supported by the United States–Israel Binational Foundation (grant 2004037) and the ERC SoftGrowth project.

Author contributions

Both authors designed the experiment. H.A. conducted the experiments and analysed the data under the supervision of E.S. Both authors wrote the manuscript.

Additional information

The authors declare no competing financial interests. Supplementary information accompanies this paper on www.nature.com/naturematerials. Reprints and permissions information is available online at http://npg.nature.com/reprintsandpermissions. Correspondence and requests for materials should be addressed to E.S.